Effects of static loads on the nonlinear vibration of circular plates

Xu, Pengpeng; Wellens, Peter

DOI
10.1016/j.jsv.2021.116111

Publication date
2021

Document Version
Final published version

Published in
Journal of Sound and Vibration

Journal of Sound and Vibration 504 (2021) 116111

Contents lists available at ScienceDirect

Journal of Sound and Vibration

journal homepage: www.elsevier.com/locate/jsv

Effects of static loads on the nonlinear vibration of circular plates

Pengpeng Xu, Peter Wellens*

Department of Maritime and Transport Technology, Delft University of Technology, Mekelweg 2, Delft 2628 CD, the Netherlands

ARTICLE INFO

Article history:
Received 1 December 2020
Revised 4 March 2021
Accepted 28 March 2021
Available online 3 April 2021

Keywords:
Nonlinear plate vibration
Static transverse load
Helmholtz–Duffing equation
Stiffening
Asymmetry
Softening

ABSTRACT

Maritime structures in water always experience a mean hydrostatic pressure. This paper investigates the nonlinear vibration of a clamped circular thin plate subjected to a non-zero mean load. A set of coupled Helmholtz–Duffing equations is obtained by decomposing the static and dynamic deflections and employing a Galerkin procedure. The static deflection is parameterized in the linear and quadratic coefficients of the dynamic equations. The effects of the static load on the dynamics, i.e. stiffening, asymmetry and softening, are investigated by means of the numerical solution of the coupled multi-mode system. An analytical solution of the single-mode vibration near primary resonance is derived. The analytical solution provides a theoretical explanation and quick quantification of the influence of the static load on the dynamics. The numerical and analytical results compare well, especially for lower values of the static deflection, confirming the effectiveness of the analytical approach. The proposed analysis method for plate vibration can be applied to other structures such as beams, membranes and combination forms.

1. Introduction

Maritime structures in water are always exposed to a mean load in the form of the hydrostatic pressure. Thin plate structures subjected to complex loads in water are likely to undergo a moderate-to-large static deflection with an amplitude of the same order as the plate thickness. The corresponding dynamic behavior differs from that of a plate not statically loaded.

There are numerous prior studies on the nonlinear dynamics of plates with static in-plane pre-loads. An early study on nonlinear vibratory properties of circular plates with initial deflection is attributed to Yamaki et al. [1], which models the nonlinear dynamics of clamped circular plates without damping that are initially stretched and compressed in the radial direction. Natural frequencies of free vibrations and the frequency-response in terms of harmonics, sub-harmonics, and super-harmonics are formulated analytically and solved numerically. The result is validated against an experiment in Yamaki et al. [2]. Later, the methodology was also adapted and applied to rectangular plates [3,4].

Hui [5,6] investigate the influence of imperfections on the dynamics of plates. The imperfection is modeled as a perturbation, and the asymptotic solution clearly shows the physical properties of the primary vibrations. Eslami and Kandil

* Corresponding author.
E-mail address: p.r.wellens@tudelft.nl (P. Wellens).

https://doi.org/10.1016/j.jsv.2021.116111

[7] extend a similar analysis to orthogonal panels, of which the primary and secondary modes were found and studied. [8,9] investigate the interaction of multiple modes of a rectangular plate vibrating under in-plane pre-loads. Their numerical results show branching in the frequency-imperfect amplitude-curve. Quasi-degeneracy phenomena that modal frequency curves avoid crossing and coalesce are observed in the secondary imperfection mode. Rotary inertia effects are discussed in Chen and Shabana [10]. The thermal effect is studied by Amabili and Carra [11]. Direct numerical solutions and numerical simulations are studied in Hui [12], Singh et al. [13], Amabili [14], Touzé et al. [15], Zarei and Khosravifard [16]. The stability of the buckling path and vibrations of in-plane pre-compressed circular plates are analyzed in Zhou et al. [17], where nonlinearity is tackled by expanding coefficients and solving the eigenvalue problem of a set of algebraic equations. Guojun and Huijian [18], Du and Ma [19] investigate the effects of static loads on the vibrations of circular sandwich plates, in which the eigenvalue problem is solved by a modified iteration method.

Another research angle is to study shallow spherical shells or plates being curved because the curvature can be seen as static deformation. Over the years, many studies have contributed to the modeling of nonlinear shells and panels with curvatures, pre-loads, and imperfections [20–27]. A comprehensive introduction to the nonlinear vibrations of plates and shells can be found in Amabili [28].

Few studies have concentrated on plate vibrations under transverse static load. [29] analyzes the effect of transverse dead loads in rectangular plate dynamics. It shows that the dead loads increase the natural frequencies. Amabili [30] compares numerical and experimental results for large-amplitude vibrations of a circular cylindrical panel. The results show the asymmetry in the vibratory amplitude in the positive and negative direction. [31] investigate the nonlinear vibration characteristics of a rotating plate under static loads in a magnetic field. An ordinary differential equation is adapted to a Duffing-like equation by introducing perturbations in the nonlinear terms. A multi-time-scale method delivers the approximated analytical solution that clearly shows the frequency shift and the response asymmetry. The numerical results are only valid for the primary mode of vibration, and the perturbations used to transform the equation could not be interpreted physically. Wang et al. [32] study the vibroacoustic behavior of a rectangular plate with imperfections subjected to a static point load. More recently, the changes of nonlinear frequencies and modes of beam [33,34] and shell [35,36] due to large deformations in nonlinear vibrations are investigated with the Carrera Unified Formulation [37,38].

The Helmholtz–Duffing equation is closely related to the nature of nonlinear plate vibrations subjected to complex transverse loads (see Section). The quadratic stiffness makes this category of nonlinear differential equations special. Chen et al. [39] extends the elliptic Lindstedt-Poincaré (ELP) method to solve strongly quadratic nonlinear oscillators with perturbed damping and stiffness. Hu [40], 41] solve free vibrations of conservative free oscillators with weakly quadratic terms with the harmonic balance method (HBM) and an auxiliary sign function in positive and negative direction. Leung and Guo [42] deploys the homotopy perturbation technique introduced in He [43], which also assumes two half-solutions, to solve Helmholtz–Duffing equations. Compared to numerical results, the homotopy perturbation generates smaller errors than [40,41]. Yeasmin et al. [44] develops a single solution to free oscillators with moderate-to-strong nonlinearity, where a modified harmonic balance method reduces the algebraic complexity. Exact solutions based on Jacobi elliptic functions are given by Zhu [45] for the Helmholtz equation, and [46] for the Helmholtz–Duffing equation.

Most studies mentioned above are about the free Helmholtz or Helmholtz–Duffing oscillator. The forced vibration of quadratic and mixed nonlinear Duffing equations has received increased attention in recent years. Jiang et al. [47] demonstrate the softening effect of nonlinear quadratic systems and compares different analytical approaches. Gusso and Pimentel [48] improves the approximation to the analytical solution of the forced Helmholtz–Duffing equation. The approximation can be further improved by a one-step correction, as proposed in Zhou et al. [49].

Little quantitative information is available on changes in structural dynamics due to uniformly distributed transverse static loads and its relation with the Helmholtz–Duffing equation, which motivates the authors to revisit the forced vibration of edge-clamped circular plates. Other popular cases, in-plane pre-loads and imperfections for example, are out of the scope of this research. Stiffening, asymmetry and softening are investigated by decomposing the total displacement in the equations of motion and isolating the static deflection before including its effect in the system of dynamic equations. The system is solved numerically, and parameters are varied systematically to demonstrate the influence of the static deflection on the dynamic properties. A HBM-based analytical solution is then derived to give immediate insight into the mechanism behind, and a quick quantification of the effect of static deflection on the dynamics of the plate. The analytical solution is compared to the numerical results.

2. Problem statement

2.1. Governing equations

Consider an isotropic homogeneous circular plate subjected to a uniformly distributed transverse load, whose lateral section is sketched in Fig. 1. The load has a non-zero static part and a dynamic part. The vibration will occur around the mean deflection that results from the static load. Table 1 gives the parameters relevant to the plate's mechanics.

We follow von Kármán nonlinear plate theory that tackles the geometrical nonlinearity associated with moderate deflection. The bending stiffness of the plate is calculated as $D = \frac{E\delta^3}{12(1-\nu^2)}$. The dynamic part of the in-plane deflection is neglected because the in-plane transient changes are small compared to the transverse ones. In this axisymmetric case, the governing

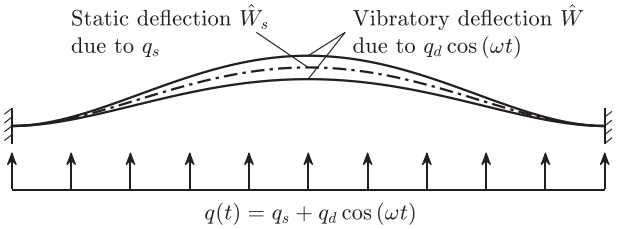

Fig. 1. Lateral view of a clamped circular plate under a uniform transverse load. The total load is decomposed into a static and a dynamic part. The plate vibrates around the mean deflection.

Table 1
Symbols for the plate model.

Symbol	Description	Value	Unit
ρ	Density	7.78	kg m^{-2}
E	Young's modulus	210	GPa
ν	Poisson ratio	0.31	
δ	Thickness	0.001	m
R	Radius	0.1	m
D	Bending stiffness	18.44	Pa
c	Damping coefficient	0.02	
Ω_0	First linear EF	1572.7	rad s^{-1}
r	Radial coordinate		m
t	Time coordinate		s
u	In-plane displacement		m
w	Transverse displacement		m

equations are given in terms of the plate displacement field in polar coordinates [50,51]. The compatibility equation then reads

$$u_{,rr} + \frac{1}{r}u_{,r} - \frac{u}{r^2} + w_{,r}w_{,rr} + \frac{1-\nu}{2r}w_{,r}^2 = 0, \tag{1}$$

where commas in subscripts denote partial differentiation in space while dots above parameters denote partial differentiation in time.

The transverse load is uniformly distributed with a static and a time-varying part $q(t) = q_s + q_d \cos(\omega t)$, with ω the frequency of oscillation. The equilibrium equation is given by

$$D\nabla^2\nabla^2 w + \rho\ddot{w} + 2c\rho\Omega_0\dot{w} - [q_s + q_d\cos(\omega t)] - \frac{E\delta}{1-\nu^2}\left(u_{,r}w_{,rr} + \frac{3}{2}w_{,r}^2 w_{,rr} + \frac{\nu}{r}uw_{,rr} + \frac{1+\nu}{r}u_{,r}w_{,r} + u_{,rr}w_{,r} + \frac{1}{2r}w_{,r}^3\right) = 0. \tag{2}$$

Here, the bi-Laplacian operator in polar coordinates is defined as $\nabla^2\nabla^2 = \frac{\partial^4}{\partial r^4} + \frac{2}{r}\frac{\partial^3}{\partial r^3} - \frac{1}{r^2}\frac{\partial^2}{\partial r^2} + \frac{1}{r^3}\frac{\partial}{\partial r}$.

The boundary conditions of the rigidly clamped plate are imposed at the plate's edge as

$$u(r,t) = 0, \quad w(r,t) = 0, \quad w_{,r}(r,t) = 0, \tag{3}$$

and at the center as

$$|u(0,t)| < \infty, \quad |w(0,t)| < \infty. \tag{4}$$

The variables are rewritten to non-dimensional form for generality. The new independent variables are ξ and τ and the new dependent $U(\xi,\tau)$ and $W(\xi,\tau)$.

$$\xi = \frac{r}{R}, \quad W = \frac{w}{\delta}, \quad U = \frac{uR}{\delta^2}, \quad \Omega = \frac{\omega}{\Omega_0}, \quad \tau = \Omega_0 t, \tag{5}$$

in which Ω_0 is the first eigenfrequency (EF) of the plate calculated by

$$\Omega_0 = \frac{\lambda_1^2}{R^2}\sqrt{\frac{D}{\rho}}, \tag{7}$$

and λ_1 (see [52]) is the first ($n = 1$) root of the system

$$\mathrm{J}_0(R\lambda_n)\mathrm{I}_1(R\lambda_n) + \mathrm{I}_0(R\lambda_n)\mathrm{J}_1(R\lambda_n) = 0, \tag{8}$$

where J and I stand for Bessel functions of the first and second kind. The non-dimensional form of Eqs. (1)–(4) now reads

$$U_{,\xi\xi} + \frac{U_{,\xi}}{\xi} - \frac{U}{\xi^2} + W_{,\xi}W_{,\xi\xi} + \frac{1-\nu}{2\xi}\left(W_{,\xi}\right)^2 = 0, \tag{9}$$

$$D\delta\nabla_\xi^2\nabla_\xi^2 W + \rho R^4\delta\Omega_0^2\ddot{W} + 2cR^4\delta\rho\Omega_0\dot{W} - R^4[q_s + q_d\cos(\Omega\tau)] - \frac{E\delta^4}{1-\nu^2}\left(U_{,\xi}W_{,\xi\xi} + \frac{3}{2}W_{,\xi}^2W_{,\xi\xi} + \frac{\nu}{\xi}UW_{,\xi\xi} + \frac{1+\nu}{\xi}U_{,\xi}W_{,\xi} + U_{,\xi\xi}W_{,\xi} + \frac{1}{2\xi}W_{,\xi}^3\right) = 0, \tag{10}$$

$$U(1,\tau) = 0, \quad W(1,\tau) = 0, \quad W_{,\xi}(1,\tau) = 0, \tag{11}$$

$$U(0,\tau) \neq \infty, \quad W(0,\tau) \neq \infty. \tag{12}$$

2.2. Proposed approach

The static component of the external load causes a static deflection. Such a static load and its resultant deflection will change the dynamic properties in the nonlinear model. Increasing the static deflection can cause stiffening and softening of the plate. Also the vibrations cause stiffening and softening, depending on whether the motion phase works towards increasing or decreasing the deflection, respectively. This effect will result in an asymmetric dynamic solution of the vibration amplitudes.

There is no direct analytical solution to the dynamic system described by Eqs. (9)–(12) that can isolate the effect of the static deflection on the dynamics of the plate. Therefore, we propose to modify the equation. The static deflection is calculated first and then combined with the - still unknown - dynamic displacement. The dynamic displacement oscillates around the mean position that is the static deflection. The combination of static deflection and dynamic deflection is the total deflection. The substitution of the total deflection into the system for the plate reveals how the plate dynamics change when the static deflection changes. The proposed approach yields a set of Helmholtz–Duffing equations with quadratic terms that depend on the static deflection, see Section 3.3.

2.3. Initial deflection

Over decades, academia proposed different analytical expressions of the static deflection subjected to a transverse load. Examples include solutions by assuming deflection shapes and/or slopes [53], the perturbation method [54], the energy minimization approach [55,56], the fracture mechanics approach [57,58]. In this work, authors choose the solution give by Zhang [59], which builds on Timoshenko's assumption. The reason for this choice is that (a). the assumed transverse shape is identical to the first basis function that is going to be applied in our dynamic analysis Eq. (21) and (b). the in-plane displacement suffices the compatibility relationship Eq. (1). In absence of in-plane pre-strain, the transverse deflection $W_s(r)$ due to the uniformly distributed transverse load q_s is given by:

$$W_s(\xi) = \hat{W}_s\left(1-\xi^2\right)^2, \tag{13}$$

where the amplitude of static deformation $\hat{W}_s$ is readily solved as a function of the transverse static load q_s

$$\hat{W}_s + \left(0.4118 + 0.25\nu - 0.16088\nu^2\right)\hat{W}_s^3 = \frac{q_s R^4}{64D\delta}. \tag{14}$$

The curve in Fig. 2 shows the dependence of dimensional $\hat{w}_s$ and dimensionless $\hat{W}_s$ on q_s within in a load range under laboratory conditions, for the plate parameters given in Table 1. In the remainder of the article the static load q_s is no longer used; instead we will use the static deflection amplitude $\hat{W}_s$ in the equations to refer to the effect of the static load.

The corresponding in-plane static deflection can be solved through substituting Eqs. (13) into (9),

$$U_s(\xi) = \hat{W}_s^2\left[\frac{\nu-7}{6}\xi^7 + \frac{10-2\nu}{3}\xi^5 + (\nu-3)\xi^3 + \frac{5-3\nu}{6}\xi\right]. \tag{15}$$

3. Dynamic model

3.1. Decomposition of deflection

The total deflection is composed of the static and the dynamic deflection:

$$U_T(\xi,\tau) = U(\xi,\tau) + U_s(\xi), \tag{16}$$

$$W_T(\xi,\tau) = W(\xi,\tau) + W_s(\xi), \tag{17}$$

where subscripts $(\cdot)_T$ denote "total". Terms without subscript are the dynamic in-plane and transverse deformation to solve for.

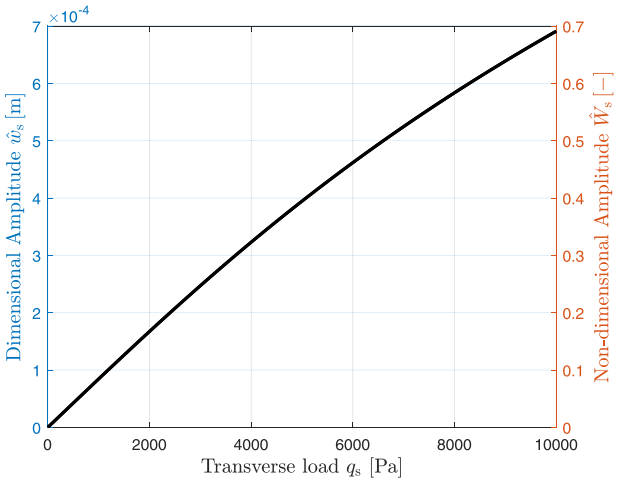

Fig. 2. Amplitude of static deflection as a function of the transverse static load.

With the total deformation, Eqs. (9) and (10) become

$$U_{\mathrm{T},\xi\xi} + \frac{U_{\mathrm{T},\xi}}{\xi} - \frac{U_{\mathrm{T}}}{\xi^2} + W_{\mathrm{T},\xi} W_{\mathrm{T},\xi\xi} + \frac{1-\nu}{2\xi}\left(W_{\mathrm{T},\xi}\right)^2 = 0, \tag{18}$$

$$\begin{aligned}\mathcal{L}(U_{\mathrm{T}}, W_{\mathrm{T}}) = {} & D\delta\nabla_\xi^2\nabla_\xi^2 W_{\mathrm{T}} + \rho R^4\delta\Omega_0^2\ddot{W}_{\mathrm{T}} + cR^4\delta\Omega_0\dot{W}_{\mathrm{T}} - R^4 q_{\mathrm{d}}\cos(\Omega\tau) \\ & - \frac{E\delta^4}{1-\nu^2}\left(U_{\mathrm{T},\xi}W_{\mathrm{T},\xi\xi} + \frac{3}{2}W_{\mathrm{T},\xi}^2 W_{\mathrm{T},\xi\xi} + \frac{\nu}{\xi}UW_{\mathrm{T},\xi\xi} + \frac{1+\nu}{\xi}U_{\mathrm{T},\xi}W_{\mathrm{T},\xi} + U_{\mathrm{T},\xi\xi}W_{\mathrm{T},\xi} + \frac{1}{2\xi}W_{\mathrm{T},\xi}^3\right) = 0.\end{aligned} \tag{19}$$

Note in Eq. (19) that the entire equation on the right-hand side of the first equal sign is being referred to as an operation $\mathcal{L}$ of U_{T} and W_{T}.

3.2. Separation of variables

The unknowns are separated into time-dependent and space-dependent parts and truncated to N

$$W(\xi,\tau) = \sum_{n=1}^{N}[\phi_n(\tau)\eta_n(\xi)], \tag{20}$$

with time-dependent part ϕ_n and space-dependent η_n. In addition, the transverse deflection is expressed in terms of polynomial basis functions (BF) [50]

$$\eta_n(\xi) = \left(1-\xi^2\right)^2\xi^{2n-2}, \quad n = 1,\ldots,N. \tag{21}$$

The exact expressions of eigenmodes (EM) are not applied in the present work because the purpose of this paper is to investigate the plate vibration where the time-dependent behavior is the key thing to solve for; polynomial BFs simplify solving the spatial differential equations and performing the Galerkin procedure. A specific EM can be constructed by assembling the chosen basis functions with coefficients that can be computed from a L^2 projection [60]. Fig. 3 illustrates EMs that are composed of basis functions up to $N = 3$ and 4.

The in-plane deformation is obtained from substituting Eqs. (20) into (18) and solving the second-order differential equation.

3.3. Dynamic equations

Substitution of Eq. (20) and the expression for U into Eq. (19) yields a partial differential equation in time τ and space ξ. The standard Galerkin procedure is applied. We obtain

$$\int_0^1 \mathcal{L}(W,U)\,\eta_n\,\xi\,\mathrm{d}\xi \quad \text{for } n = 1,\ldots,N. \tag{22}$$

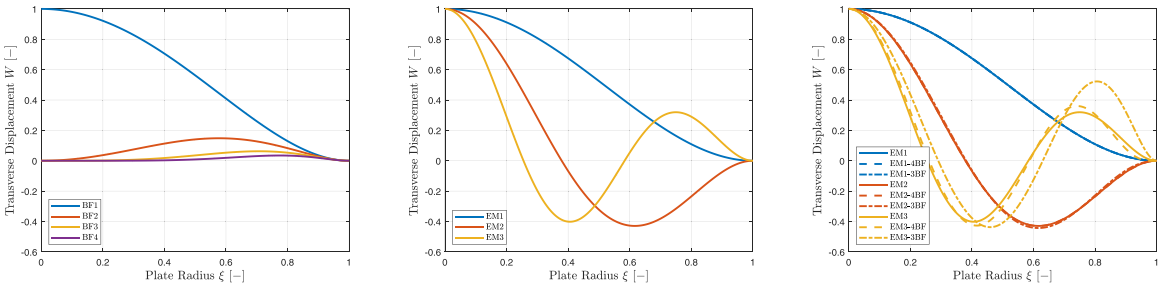

(a) Basis functions (b) Exact EM (c) Combination

Fig. 3. Examples of basis functions (BF) and eigenmodes (EM). (a) Polynomial BF; (b) Exact EM; (c) comparison between exact EM and EM shapes constructed by three or four basis functions.

Performing the integration generates a set of N coupled second-order ordinary differential equations with respect to τ

$$\sum_{k=1}^{N} c_{1nk}\ddot{\phi}_k + \sum_{k=1}^{N} c_{2nk}\dot{\phi}_k + \sum_{k=1}^{N} c_{3nk}\phi_k + \sum_{k,i=1}^{N} c_{4nki}\phi_k\phi_i + \sum_{k,i,j=1}^{N} c_{5nkij}\phi_k\phi_i\phi_j + c_{6n}q_{\mathrm{d}}\cos(\Omega\tau) + c_{7n} = 0 \quad \text{for } n = 1,\ldots,N. \tag{23}$$

The dynamic system (23) can be categorized as a set of coupled, forced Helmholtz–Duffing oscillators. Coefficients c are determined with the Galerkin procedure. The c_{1nk} stand for the inertial coefficients, c_{2nk} for the damping, c_{3nk} for the linear stiffness, c_{4nki} for the quadratic stiffness and c_{5nkij} for the cubic stiffness. The c_{6n} are the coefficients of the dynamic load. Coefficients c_{7n} are constants containing $\hat{W}_{\mathrm{s}}$ and $\hat{W}_{\mathrm{s}}^3$ originating from the static deflection. This term is balanced with the initial static transverse load q_{s} in Eq. (2). It is worth emphasizing that the asymmetry of the dynamic system is not caused by c_7. Instead, the quadratic dynamic terms will result in constant terms that lead to asymmetry in the solution, which will be demonstrated in the sections following up.

4. Numerical solution to the coupled multi-mode system in a large range of frequency

Fig. 3 c compares exact eigenmodes and the approximations constructed by the combination of basis functions. It indicates that using $N = 3$ gives a good approximation of the first and second eigenmode but an unsatisfactory approximation of the third. Higher modes and/or higher accuracy can be obtained when more polynomial basis functions are included. Because four terms give a only a marginal improvement of the representation of the first two eigenmodes at the expense of a three-fold increase in computational effort, hereafter all computations are performed with $N = 3$ in polynomial expression (20).

The numerical computation is performed with dimensionless variables, which are based on the dimensional parameters stated in Table 1. We have varied the static deflection W_{s}; and for each static deflection, we have varied the frequency Ω of the dynamic load. The numerical integration and the frequency variation are carried out with MatCont [61]; that is a MATLAB®-based package that utilizes continuation techniques [62] and the ode45 solver for the numerical time integration. Only steady-state results in the presence of damping are reported.

4.1. Trajectories in the state-space representation

Fig. 4 illustrates the trajectories of the steady-state of the dynamic variable ϕ_n with different static deflections under the external excitation. The excitation amplitude is fixed at $q_{\mathrm{d}} = 500$ and the static deflection varied as $\hat{W}_{\mathrm{s}} = 0.0,\ 0.1$ and 0.2 in different rows. The excitation frequency is $\Omega = 1.125$ corresponding to the fold region in Figs. 5 and 6. In this region, there are three solutions, two stable and one unstable. The first two columns of the figure are for the state space representation of the first and second BF in the polynomial of the dynamic deflection W. The third column shows 3D plots that compare the dynamic displacement amplitudes of the first three BFs. It is worth noting that the trajectories appear to cross themselves in the projection towards lower dimensions shown in the second column of Fig. 4, but that they are not crossed in the six-dimensional phase portrait $\left(\phi_1, \dot{\phi}_1, \phi_2, \dot{\phi}_2, \phi_3, \dot{\phi}_3\right)$.

Fig. 4 has evidence of the effects of stiffening and of asymmetry on the dynamic response amplitude induced by static deflections. Without static deflection, a harmonic excitation generates centro-symmetric trajectories in state space. Stiffening becomes apparent from the extremities of the curves becoming smaller for larger values of the static deflection. Asymmetry is apparent from the centroids of the curves shifting along the horizontal axis, particularly for the positive position half-plane of the second BF being different in the opposing position half-plane. Later, we will also see that, besides stiffening and asymmetry, the static deflection causes softening - softening is not shown straightforwardly by these trajectories.

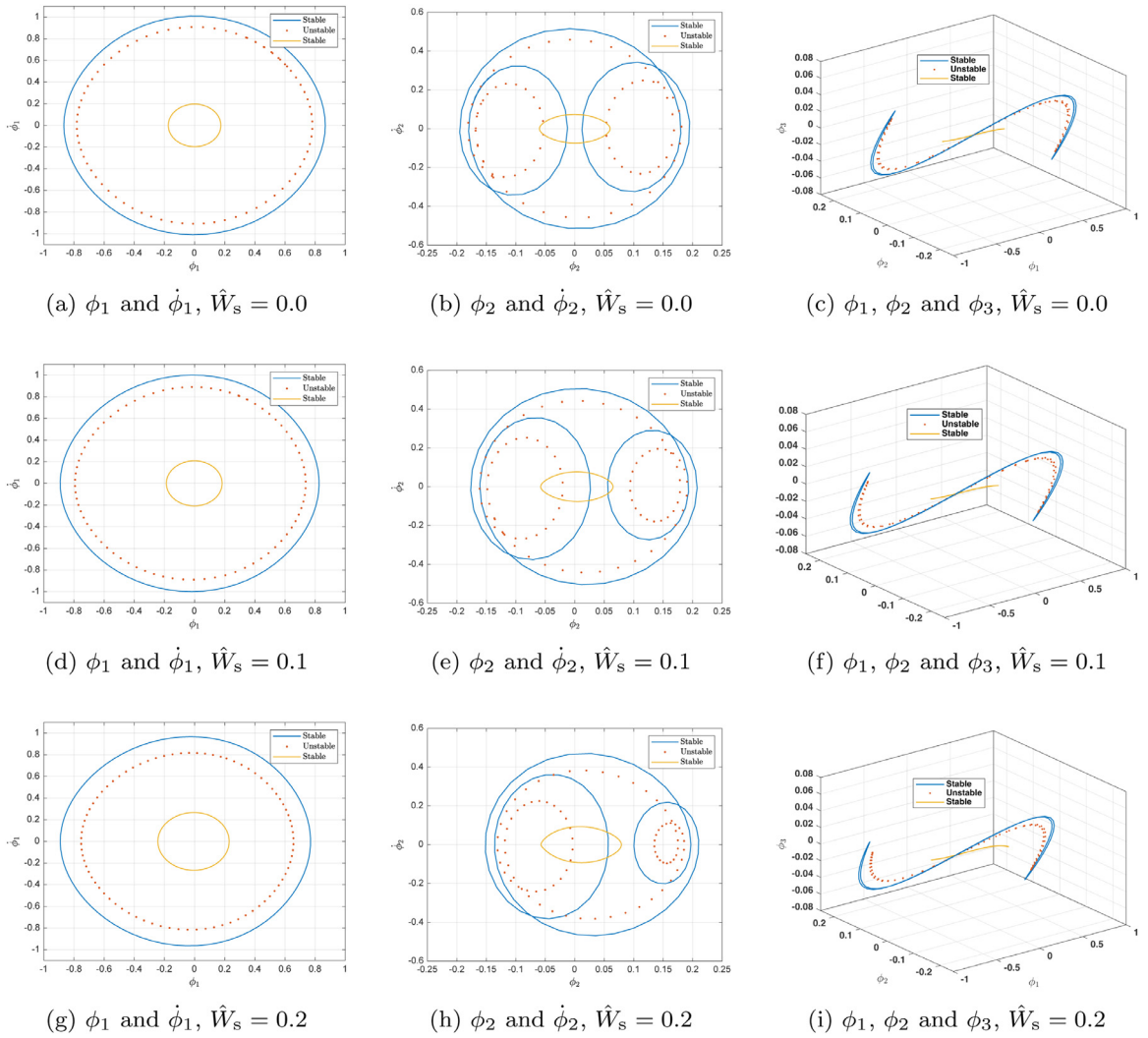

(a) ϕ_1 and $\dot{\phi}_1$, $\hat{W}_\mathrm{s} = 0.0$ (b) ϕ_2 and $\dot{\phi}_2$, $\hat{W}_\mathrm{s} = 0.0$ (c) ϕ_1, ϕ_2 and ϕ_3, $\hat{W}_\mathrm{s} = 0.0$

(d) ϕ_1 and $\dot{\phi}_1$, $\hat{W}_\mathrm{s} = 0.1$ (e) ϕ_2 and $\dot{\phi}_2$, $\hat{W}_\mathrm{s} = 0.1$ (f) ϕ_1, ϕ_2 and ϕ_3, $\hat{W}_\mathrm{s} = 0.1$

(g) ϕ_1 and $\dot{\phi}_1$, $\hat{W}_\mathrm{s} = 0.2$ (h) ϕ_2 and $\dot{\phi}_2$, $\hat{W}_\mathrm{s} = 0.2$ (i) ϕ_1, ϕ_2 and ϕ_3, $\hat{W}_\mathrm{s} = 0.2$

Fig. 4. Comparison of trajectory projections in the fold region ($\Omega = 1.125$) with different static deflection $\hat{W}_\mathrm{s} = 0.0$, 0.1 and 0.2. The transverse dynamic load is fixed, $q_\mathrm{d} = 500$.

4.2. Frequency-response curves for basis functions with different static deflections

Fig. 5 shows the frequency response (FR) of the first three BFs in three different rows for different values of the static deflection in each plot. The amplitudes of BF1, BF2, and BF3 become large near the first, second, and third eigenfrequency, respectively. The quadratic terms in the system of Duffing equations Eq. (23) lead to asymmetry in the dynamic solutions. Therefore, it is necessary to show both the maximum positive deflection of the plate and the maximum negative deflection. The negative deflection amplitudes are shown in the second column of Fig. 5, in which particularly the negative value of the left-most peak of BF1 is different from the positive value. Also, note that the sign of BF2 is always opposite to BF1 and BF3 due to the construction of the EM. Enlargements of the areas in Fig. 5 indicated by A to F are shown in Fig. 6.

4.2.1. Stiffening, asymmetry, and softening effects of static deflections

The aforementioned three changes in vibratory behavior due to $\hat{W}_\mathrm{s}$ are more clearly visualized in Fig. 6b, c, f: the stiffened effect increases the eigenfrequencies and shifts the FR curves towards higher frequencies; the asymmetry decreases the positive amplitudes but increases the negative; the softening effect adjusts the originally rightward-bending FR curves, and bends them leftward. The increased stiffness also becomes apparent from the lower FR amplitudes for higher values of the static deflection. All three effects are proportional to the static deflection.

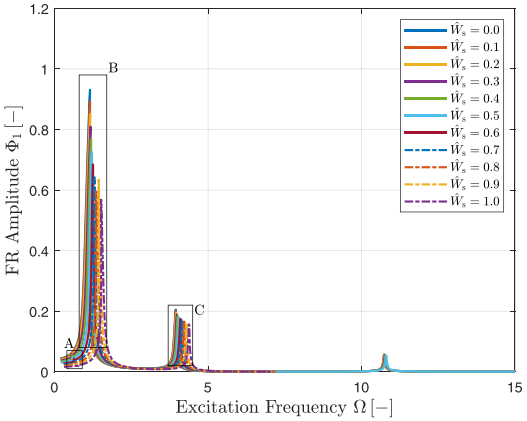

(a) BF1 Positive

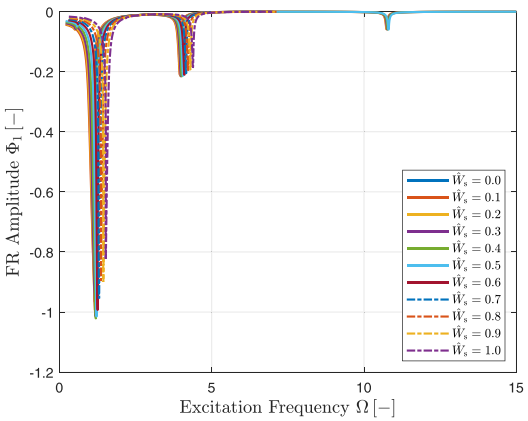

(b) BF1 Negative

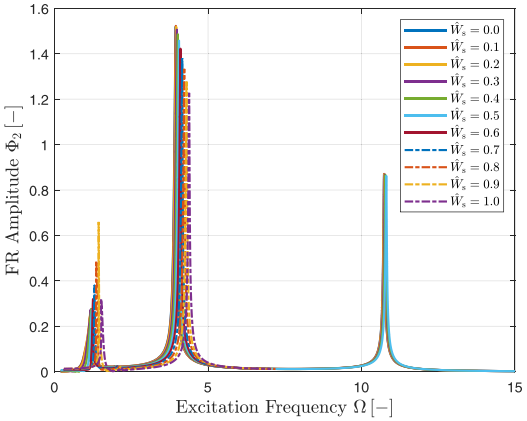

(c) BF2 Negative

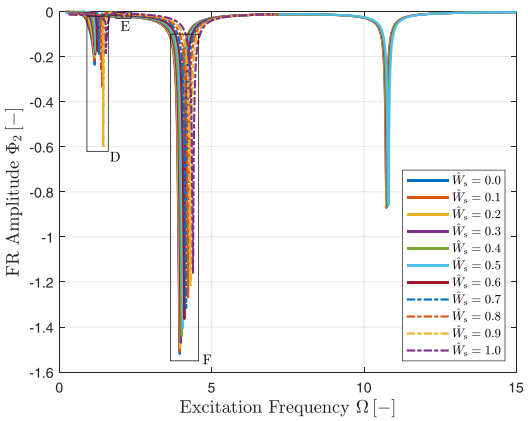

(d) BF2 Positive

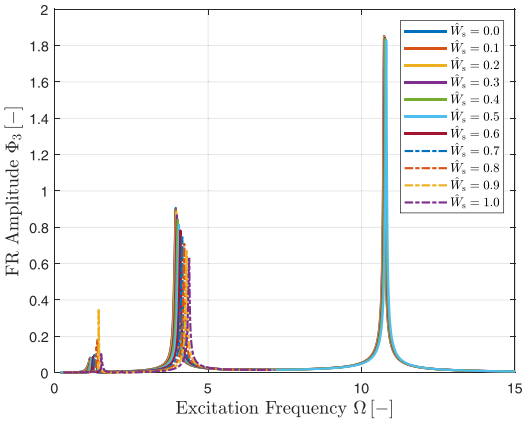

(e) BF3 Positive

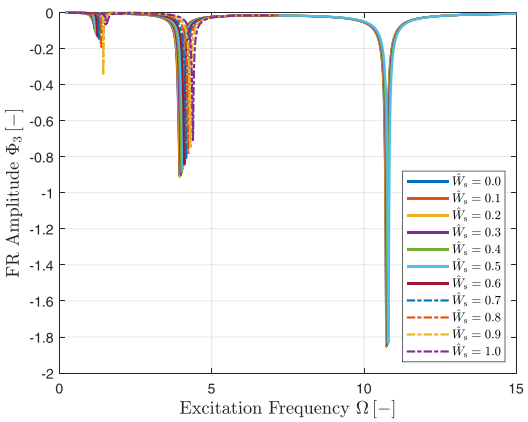

(f) BF3 Negative

Fig. 5. Frequency-response curves of the first three basis functions (BF) with different static deflections. The transverse dynamic load is fixed, $q_d = 500$. The left column shows the positive deflection maxima. The right column shows negative deflection maxima. Enlargements A to F are shown in Fig. 6.

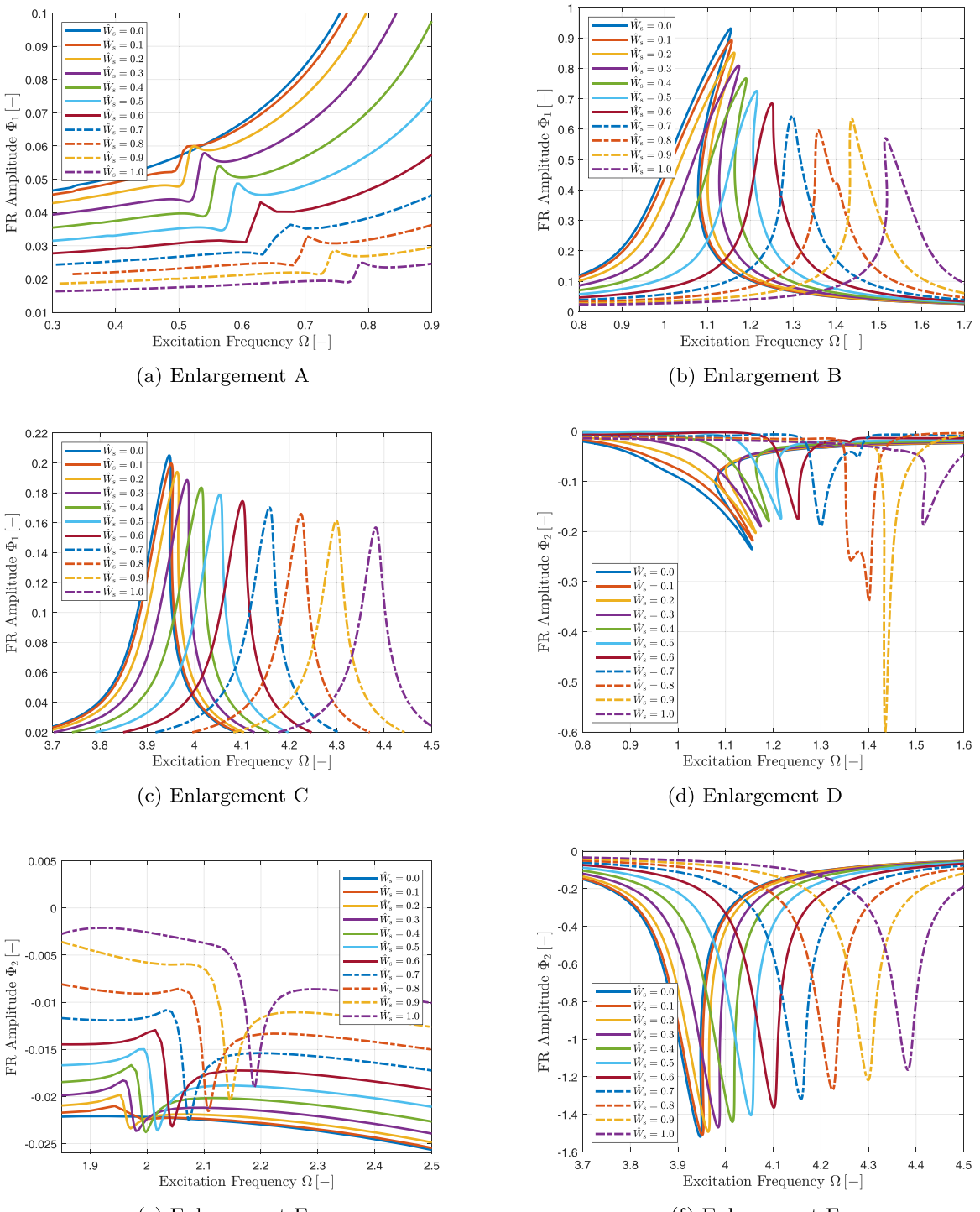

(a) Enlargement A

(b) Enlargement B

(c) Enlargement C

(d) Enlargement D

(e) Enlargement E

(f) Enlargement F

Fig. 6. Enlargements of frequency-response curves with different static deflections $\hat{W}_s$ in Fig. 5 with specific frequency ranges for basis function 1 (a, b and c) and basis function 2 (d, e and f). The dynamic transverse load is fixed, $q_d = 500$.

4.2.2. Sub- and super-harmonics

As an important representative of nonlinearity, sub-harmonics are visible in the numerical results. Fig. 6a, e show the $\frac{1}{2}\Omega$ sub-harmonics, which are due to the quadratic terms of BF1 and BF2 for the first and second eigenfrequency. Interesting illustrations are Fig. 6b, d, in which the $\frac{1}{3}\Omega$ sub-harmonics of BF2 for the secondary resonance are close to the harmonics of the primary resonance. That these two peaks approach each other for increasing static deflection is evident at $\hat{W} = 0.8$;

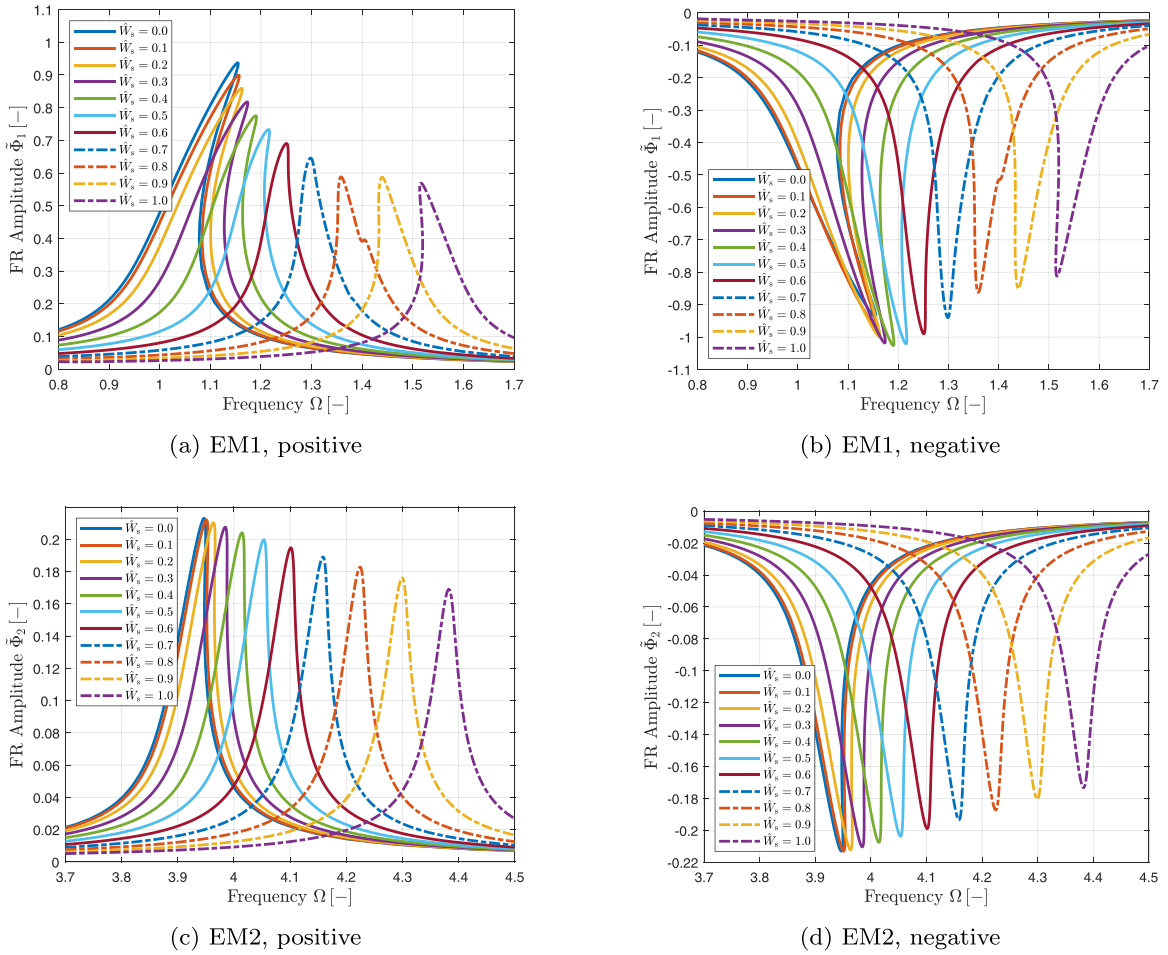

Fig. 7. FR curves of the first and second eigenmode obtained from the numerical results. The dynamic transverse load is fixed, $q_d = 500$. These eigenmode-based results are computed from the BF-based results shown in Fig. 5.

the peaks merge when $\hat{W}_s = 0.9$, which amplifies the response amplitudes. The present work does not detect the super-harmonics, the counterpart of sub-harmonics, because of the relatively high damping ratio.

4.3. Transfer to eigenmodes from basis functions

The analysis so far was based on BFs (see Eq. (21)). The results in terms of eigenmodes (EM) can be calculated by transferring the BF-based frequency response (FR) ϕ to the EM-based FR $\tilde{\phi}$ utilizing the L2 projection. The EM amplitude is denoted as $\tilde{\Phi}$.

A three-term combination of polynomial BF only gives satisfactory accuracy up to the second EM (see Section 3.2) and the second EF (see [1]). Therefore, we analyze the first and second eigenmodes and leave the third out of the discussion. Fig. 7 shows FR curves based on the EMs. Three influences of static deflection - stiffening, asymmetry and softening - are visible in a similar way as in Figs. 5 and 6.

Backbones (BB) of the FR, representing the asymptotes of the theoretical undamped eigenfrequencies, depicted in Fig. 8, demonstrate the static load effects in a clear overview. Backbones are obtained by linearly interpolating the cusps of the FR with varying dynamic load amplitudes, $q_d = 10$ (or 20) to 500. The well-ordered ranking of BBs demonstrates the stiffening effect; the difference in amplitudes in positive- and negative-direction is evidence of the asymmetrical effect; the change in bend-direction of EM1 shows the softening effect. The effect of the static load on stiffening is strong in both EM1 and EM2; the asymmetry is significant in EM1 and insignificant but still observable in EM2; softening hardly affects EM2.

5. Analytical solution to the single-mode system near the primary resonance

Qualitative analysis provides insight into the mechanisms behind the effect of a static load on the dynamics of the circular plate. Hence we look into an approximation to the analytic solution of a single eigenmode (EM) of a multi-mode

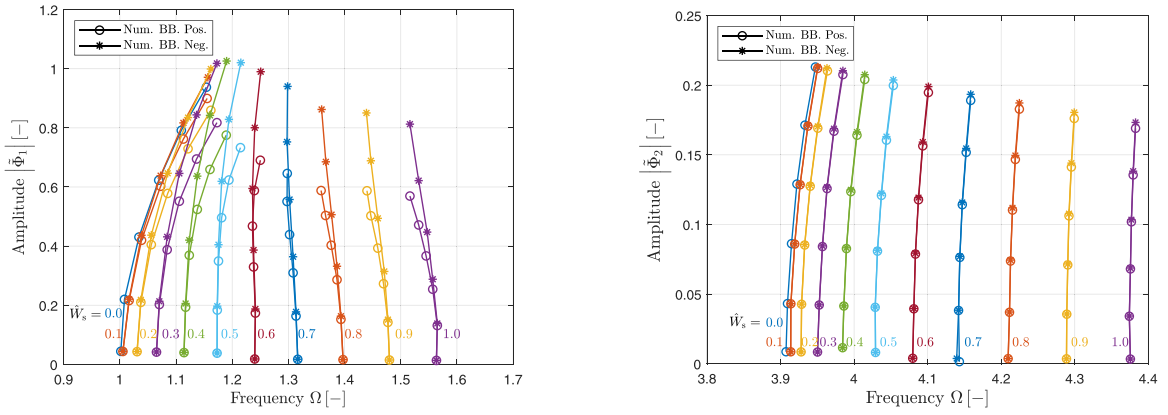

(a) EM1 (b) EM2

Fig. 8. Backbones of EM-based FR obtained from the numerical results. Both static deflection $\hat{W}_s$ and dynamic transverse load q_d are varied. For a certain backbone with fixed $\hat{W}_s$, the load amplitudes vary among $q_d = 500, 400, 300, 200, 100, 20$ (or 10).

Table 2
Coefficients of the first and second EM.

Coefficient	EM1	EM2
σ	0.04	0.04
γ	1.520274439	0.257259273
α	1.537908112	0.4013065576
β	0.502206616	0.6613560788
χ	8.856630555×10^{-5}	4.254542778×10^{-6}

system in Eq. (23) near its eigenfrequency (EF). The response of one EM will be dominant and other EMs are negligible when the load is exerted near one of the EFs. Using three polynomial terms, Eq. (20) is rewritten to

$$\tilde{W}(\xi,\tau) = \phi(\tau)\Big[z_1\big(1-\xi^2\big)^2 + z_2\big(1-\xi^2\big)^2\xi^2 + z_3\big(1-\xi^2\big)^2\xi^4\Big]. \tag{24}$$

The tilde above a variable indicates time-dependent variables associated with an EM. z_n are coefficients of basis functions to construct a particular EM, which can be explicitly calculated by the L^2 projection. Substitution of Eqs. (24) into (18) yields the in-plane EM $\tilde{U}(\xi,\tau)$.

Substitution of $\tilde{W}(\xi,\tau)$ and $\tilde{U}(\xi,\tau)$ into Eq. (19) gives a single ordinary differential eqution about $\tilde{\phi}(\tau)$ in the same form of Eq. (23). The forced Helmholtz–Duffing equation is obtained by normalising the single dynamic equation and neglecting constant terms.

$$\ddot{\phi} + \sigma\dot{\phi} + \big(1 + \hat{W}_s^2\gamma\big)\phi + \hat{W}_s\alpha\phi^2 + \beta\phi^3 = \chi q_d\cos(\Omega\tau), \tag{25}$$

The unity part in the linear term is calculated from $\frac{\lambda_1^2}{\lambda_1^2}$ (see Eq. (7)), which is the first linear EF without static deformation, and its EM. Coefficients σ, γ, α, β and χ are explicitly calculated with material parameters stated in Table 1 and coefficients z_n for a particular EM $\tilde{W}$. The static deflection $\hat{W}_s$ due to static load q_s exists in the linear and quadratic term. Table 2 lists the parameter values of Eq. (25) for the first and second EM.

Values of γ and α - values are associated with $\hat{W}_s$ - of the first EM are about six and four times that of the second EM, respectively. The effects of static deflection on the first EM are more conspicuous than those on the second. What is tested but not shown is that the cubic coefficient β is actually much larger than α for all the other EM from the third EM on. This indicates that the forced vibration of higher EMs is strongly cubic so that the quadratic is negligible. Hence we investigate the influence of the static load around primary resonance to demonstrate and estimate the static influence on the dynamics of the plate.

Truncating the Fourier expansion to the first order, the solution of Eq. (25) is assumed as

$$\phi(\tau) = A_0 + a_1\cos(\Omega\tau) + b_1\sin(\Omega\tau) \quad \text{and} \quad A_1 = \sqrt{a_1^2 + b_1^2}, \tag{26}$$

where the total amplitude is

$$A = A_0 + A_1. \tag{27}$$

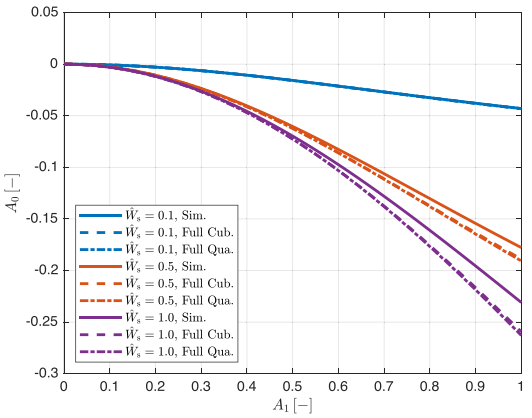

(a) A_1 and A_0

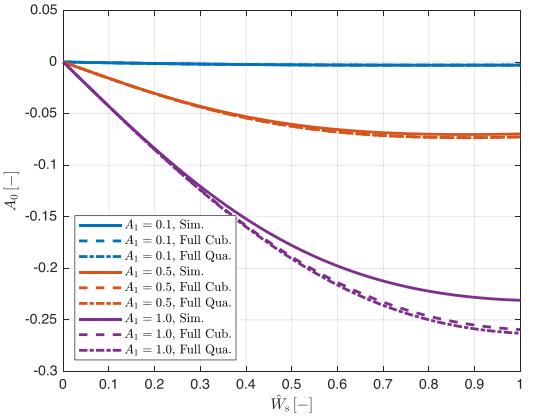

(b) $\hat{W}_s$ and A_0

Fig. 9. Comparison of approximations of Eq. (37) (Sim.), Eq. (33) (Full Cub.) and Eq. (35) (Full Qua.).

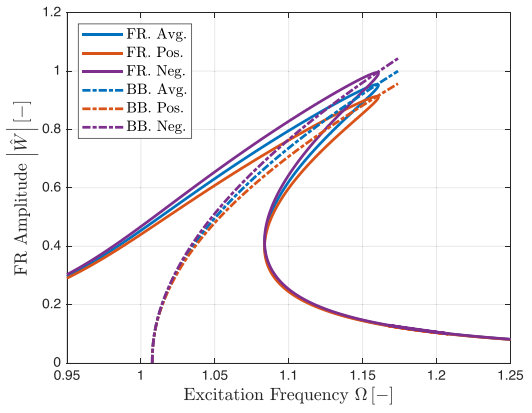

(a) $\hat{W}_s = 0.1$

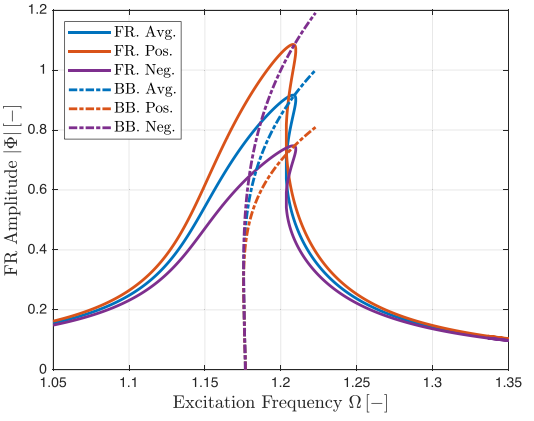

(b) $\hat{W}_s = 0.5$

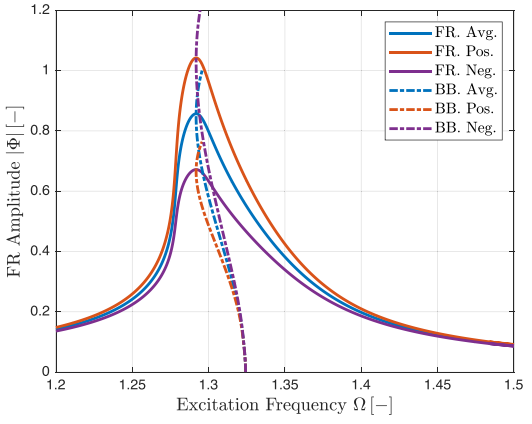

(c) $\hat{W}_s = 0.7$

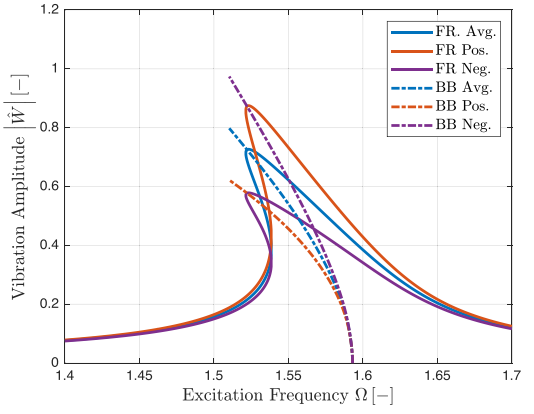

(d) $\hat{W}_s = 1.0$

Fig. 10. FRs and BBs of HBM. with different $\hat{W}_s$. Eq. (38) calculates FRs with different dynamic load q_d. Only FRs with $q_d = 500$ are shown for reasons of clarity. Interpolating the cusps of FRs generates the BBs. Correcting FRs and BBs in amplitudes with the asymmetry Eq. (35) yields curves in the positive and negative direction.

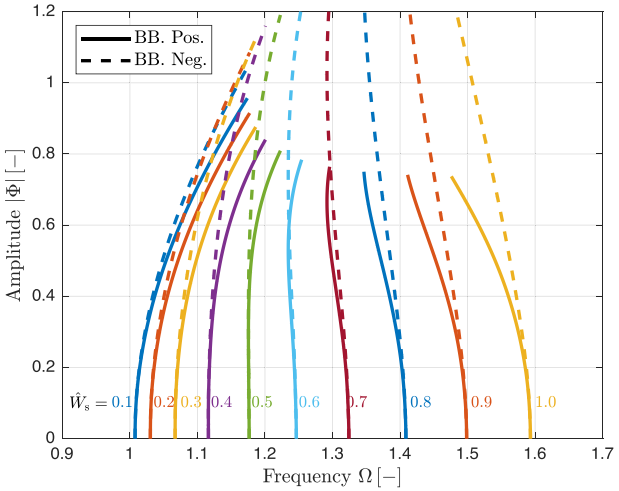

Fig. 11. Backbones of EM-based FR of analytical approximations. Both static deflection $\hat{W}_s$ and dynamic transverse load q_d are varied. For a certain backbone with fixed $\hat{W}_s$, the load amplitudes vary from $q_d = 500$ to 10.

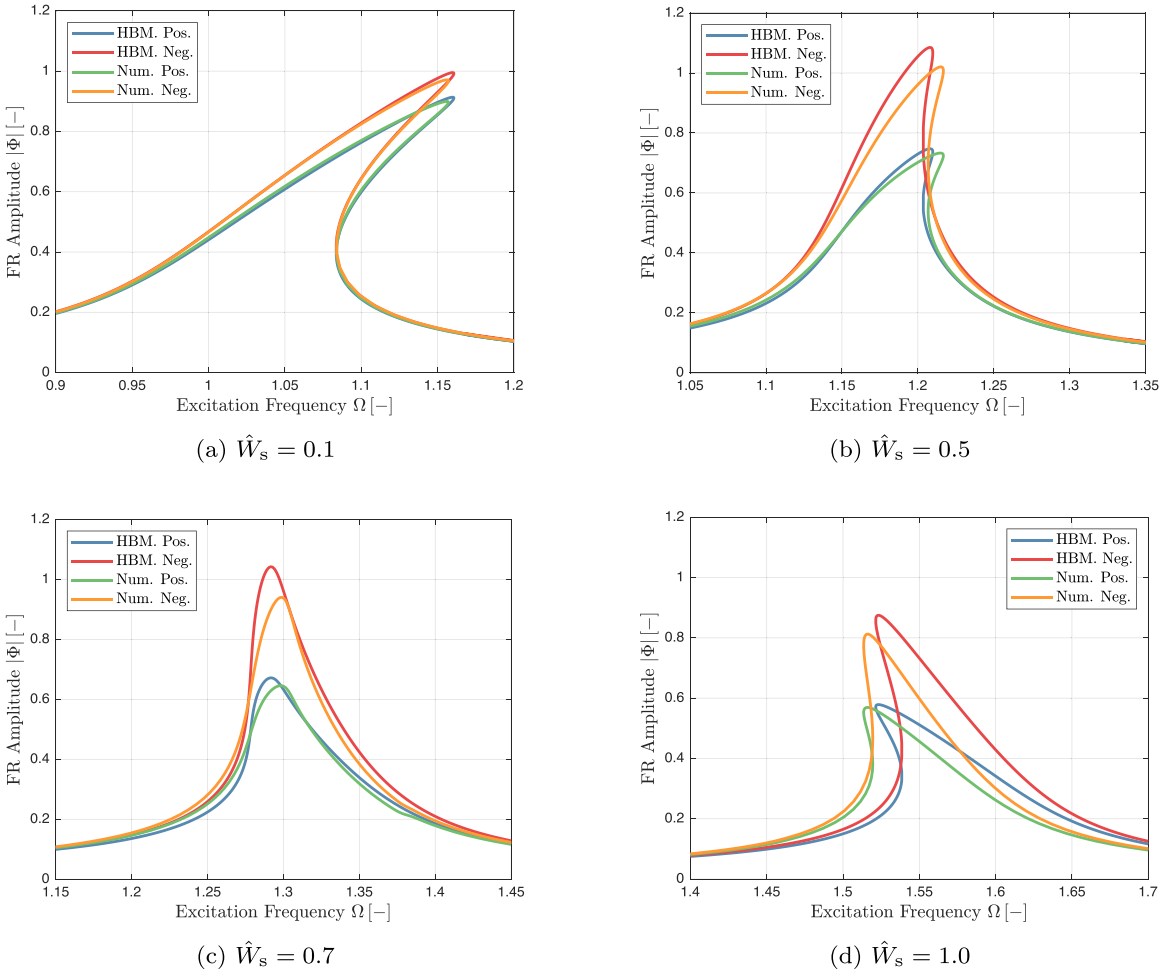

Fig. 12. Comparison of FRs of analytical approximation (HBM) and numerical method. The dynamic load is fixed at $q_d = 500$.

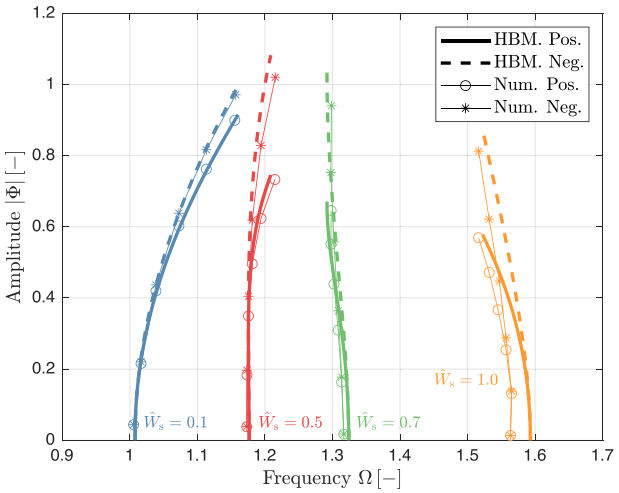

Fig. 13. Comparison of BBs of analytical approximation (HBM) and numerical method.

Proceeding with the HBM, we substitute Eqs. (26) into (25) and equate the summation of constants and coefficients of the primary harmonic to zero. The resulting equations are

$$\beta A_0^3 + \hat{W}_s \alpha A_0^2 + \left[\frac{3\beta\left(a_1^2+b_1^2\right)}{2} + \left(1+\hat{W}_s^2\gamma\right)\right]A_0 + \frac{\hat{W}_s\alpha\left(a_1^2+b_1^2\right)}{2} = 0 \tag{28}$$

$$2\hat{W}_s\alpha A_0 a_1 + \frac{3\beta a_1}{4}\left(a_1^2+b_1^2\right) - a_1\Omega^2 + \left(1+\hat{W}_s^2\gamma\right)a_1 + \sigma b_1\Omega + 3\beta A_0^2 a_1 = \chi q_d \tag{29}$$

$$2\hat{W}_s\,\alpha A_0 b_1 + \frac{3\beta b_1}{4}\left(a_1^2+b_1^2\right) - b_1\Omega^2 + \left(1+\hat{W}_s^2\gamma\right)b_1 - \sigma a_1\Omega + 3\beta A_0^2 b_1 = 0. \tag{30}$$

5.1. Stiffening

The linear coefficient in Eq. (25) determines the linear EF, which is calculated as

$$\Omega_{s0} = \sqrt{1+\hat{W}_s^2\gamma}, \tag{31}$$

in which Ω_{s0} stands for the first EF affected by the static deflection. Therefore the static deflection stiffens the plate and raises the EF regardless of the deforming direction. In case of small static deflection, the EF increases with the static deflection squared because Eq. (31) can be expanded as

$$\Omega_{s0} = 1 + \frac{\gamma}{2}\hat{W}_s^2 + O\left(\hat{W}_s^4\right). \tag{32}$$

5.2. Asymmetry

Substitution of Eq. (31) into (28) leaves us a cubic equation about A_0,

$$\beta A_0^3 + \hat{W}_s\alpha A_0^2 + \left(\tfrac{3\beta A_1^2}{2} + \Omega_{s0}^2\right)A_0 + \tfrac{\hat{W}_s\alpha A_1^2}{2} = 0. \tag{33}$$

Solving Eq. (33) and eliminating the imaginary parts from the three roots generates the solution of A_0. However, its solution is nontrivial because of the cubic nature of the equation. Alternatively, we neglect the highest power term in Eq. (33) and obtain a quadratic equation:

$$\hat{W}_s\alpha A_0^2 + \left[\tfrac{3\beta A_1^2}{2} + \Omega_{s0}^2\right]A_0 + \tfrac{\hat{W}_s\alpha A_1^2}{2} = 0. \tag{34}$$

Solving Eq. (34) and choosing the solution with physical meaning from the two gives

$$A_0 = -\frac{3{A_1}^2\beta + 2{\Omega_0}^2}{4\hat{W}_s\alpha} + \frac{\sqrt{9{A_1}^4\beta^2 - 8\hat{W}_s^2\alpha^2{A_1}^2 + 12{A_1}^2\beta{\Omega_0}^2 + 4{\Omega_0}^4}}{4\hat{W}_s\alpha}. \tag{35}$$

In case of small static deflection, the term under the square-root can be expanded as

$$\sqrt{9A_1{}^4\beta^2 - 8\hat{W}_s^2\alpha^2A_1{}^2 + 12A_1{}^2\beta\,\Omega_0{}^2 + 4\,\Omega_0{}^4} = 3A_1{}^2\beta + 2\,\Omega_0{}^2 - \frac{\hat{W}_s^2\alpha^2A_1{}^2}{3A_1{}^2\beta + 2\,\Omega_0{}^2} + O\left(\hat{W}_s^4\right). \tag{36}$$

Thus, Eq. (35) reduces to

$$A_0 \approx -\frac{\hat{W}_s\alpha A_1^2}{2\Omega_{s0}^2 + 3\beta A_1^2}. \tag{37}$$

The minus sign indicates that the asymmetry is opposite to the direction of static deflection. It implies that, subjected to a static load in positive direction, the plate's dynamic bending is larger in negative direction and smaller in positive direction. Eq. (37) is identical to the approximation obtained by Gusso and Pimentel [48] where both cubic and quadratic terms of Eq. (33) are neglected. It is also interesting to simplify Eq. (37) further to $A_0 = -\frac{\hat{W}_s\alpha A_1^2}{2\left(1+\hat{W}_s^2\gamma\right)}$ in case of $\beta \ll 1$. This approximation is identical to the solution obtained with the multi-time-scale method in Benedettini and Rega [63].

Fig. 9 compares the simplified approximation given by Eq. (37), labelled as "Sim.", the full solution to the cubic equation Eq. (33), labelled as "Full Cub.", and the approximation given by Eq. (35), labelled as "Full Qua.". The comparison shows that the simplified approximation is valid for small static deflections. As $\hat{W}_s$ increases to the moderate-to-large range $\hat{W}_s, A_1 \leqslant 1$, the simplified approximation is still acceptable with a maximum error of 7.42% at $\hat{W}_s = 1$ and $A_1 = 1$. The comparison also confirms that the quadratic approximation of Eq. (35) is accurate up to $\hat{W}_s = 1$ with an error less than 0.1%.

5.3. Softening

Cubic stiffness is the nature of geometric nonlinear hardening in plate models. Quadratic nonlinearity in the Helmholtz–Duffing equation causes softening [47,64]. This implies that the softening effect of the static deflection is a correction to the hardening effect. The correction makes the backbones (BB) bend towards lower frequencies and its strength is proportional to the static deflection, see Eq. (25).

Summing the squares of Eqs. (29) and (30) and substituting Eq. (37) leads to an implicit function $\mathcal{F}\left(\Omega, A_1; \hat{W}_s, q_d\right) = 0$

$$\begin{aligned} &A_1^2\left(\Omega^4 + \Omega_{s0}^4\right) + \frac{9\beta^2A_1^6}{16} - \frac{3A_1^4\beta\left(\Omega^2 - \Omega_{s0}^2\right)}{2} + \frac{4A_1^4\alpha^2W_s^2\left(\Omega^2 - \Omega_{s0}^2\right)}{3A_1^2\beta + 2\Omega_{s0}^2} + \Omega^2A_1^2\left(\sigma^2 - 2\Omega_{s0}^2\right) \\ &+ \frac{4A_1^6W_s^4\alpha^4}{\left(3A_1^2\beta + 2\Omega_{s0}^2\right)^2} - \frac{3A_1^6W_s^2\alpha^2\beta}{3A_1^2\beta + 2\Omega_{s0}^2} = \chi^2q_d^2. \end{aligned} \tag{38}$$

Eq. (38) generates FR curves in which $\hat{W}_s$ and q_d are parameters. Here we substitute the simplified expression Eq. (37) rather than the quadratic Eq. (35) or the cubic solution of Eq. (33) because they complicate the expression of Eq. (38) while providing only a minor improvement in accuracy (see Fig. 9).

Fig. 10 illustrates the average, positive, and negative FR and BBs with different static defection. Fig. 11 depicts BBs of more static load cases. In the moderate range, $\max(A) \approx 1$, the cubic stiffness causes rightward bending (towards higher frequencies), while the quadratic stiffness resulting from the static load bends the curves leftwards (towards lower frequencies). This softening correction increases with the static load. The coexistence of left-bending and right-bending is most pronounced around $\hat{W}_s = 0.7$. Then the softening becomes dominant over hardening. Figs. 10 and 11 also illustrate the stiffening (see Section 5.1) and the asymmetry (see Section 5.2).

5.4. Comparison with numerical results and discussion

Numerical results from Section 4.3 are used to verify the approximation derived here. Figs. 12 and 13 compare the numerical and analytical FR and BB under different static deflections. From the comparison we find that the two approaches are in good agreement for the overall trend of curves. The agreement verifies not only the hardening effect of the von Kármán plate model but also the stiffening, asymmetry, and softening effects due to the static deflections (loads). When considered in more detail, the analytical approximation, compared with numerical results, overestimates stiffening and asymmetry. As the static deflection increases, the differences between curves from the numerical and the analytical approximation grow accordingly. The differences are due to the approximations used and the fact that a single eigenmode is considered in the analytical approximation. The accuracy for a single-mode approximation to the complete system can be improved by including more terms in the Fourier series [48] and correcting the solution with multiple steps [49].

The difference in asymmetry between the numerical results and the analytical approximation are attributed to the overestimation of A_1. The asymmetry A_0 becomes larger accordingly, see Eqs. (35) and (37).

The difference in leftward or rightward bending, i.e. hardening and softening, is because of the effect of stiffening decrements (the roots of the backbones) and overestimated amplitudes (the cusps of the backbones). It can enhance or reduce the softening or hardening curves under certain conditions. In general, both the hardening and softening of the analytical

approximation are stronger than that of the analytical approximation for larger static deflections. This difference is also mainly because of the overestimation of A_1.

The analytical approximation provides a good explanation and the first estimation of the changes in dynamic behavior of the plate due to static deflection.

6. Conclusion

This paper theoretically investigates the effects of a static transverse load on the nonlinear dynamic behavior of a clamped circular plate. For generality, the variables and the governing equations have been made dimensionless. Decomposing the total deflection into a static deflection and a dynamic deflection, and parametrising the static deflection in the dynamic equations lead to a set of coupled, forced Helmholtz–Duffing equations. The linear and quadratic terms in the Helmholtz–Duffing equations are affected by the static deflection.

Numerical calculations have been performed and an analytical model has been derived to capture the effect of a moderate-to-large static load has on the transverse vibrations. Numerical results, as well as analytical results, illustrate the frequency response characteristics for different values of the static load and show its effect in the form of stiffening, asymmetry, and softening. The numerical approach for the multi-degree of freedom Galerkin system is valid for a wide range of excitation frequencies and multiple axisymmetric EM. Stiffening, asymmetry and softening due to the static load have a significant effect on the first EM and its frequency. It is also found that, for higher EM, the stiffening effect is considerable, while softening less so and that the asymmetry is negligible.

The analytical approach utilizes harmonic balancing to solve a single EM vibration near the primary resonance. The analytic solution provides a mathematical explanation and a fast approximation of the aforementioned stiffening, asymmetry and softening as a result of the static deformation. Numerical and analytical results are in good agreement for the frequency response in a range of frequencies and for the backbone curves for lower values of the static deflection. The verification of the argument is addressed by the comparable results of numerical calculation and theoretical analysis. The differences between the numerical method and the analytical approximation grow larger as the static deflection increases, but the trends remain the same.

The analytical approximation is found to be a good predictor for the effect of a static load on the nonlinear dynamic behavior of a clamped circular plate. In different cases, the relation between deflection and static loading is not unique. The present analysis has the potential of extension to those different cases. There is also a prospect to apply the proposed method in other typical models like a beam, string, and membrane.

Declaration of Competing Interest

The authors declare that they have no known competing financial interests or personal relationships that could have appeared to influence the work reported in this paper.

CRediT authorship contribution statement

Pengpeng Xu: Conceptualization, Methodology, Software, Validation, Formal analysis, Investigation, Data curation, Writing - original draft, Writing - review & editing, Visualization. **Peter Wellens:** Conceptualization, Methodology, Software, Validation, Formal analysis, Investigation, Data curation, Writing - original draft, Writing - review & editing, Supervision.

Acknowledgement

This work is financially supported by the program of China Scholarship Council (CSC) with project no. 201707720039.

References

[1] N. Yamaki, K. Otomo, M. Chiba, Non-linear vibrations of a clamped circular plate with initial deflection and initial edge displacement, part I: theory, J. Sound Vib. 79 (1) (1981) 23–42.
[2] N. Yamaki, K. Otomo, M. Chiba, Non-linear vibrations of a clamped circular plate with initial deflection and initial edge displacement, part II: experiment, J. Sound Vib. 79 (1) (1981) 43–59.
[3] N. Yamaki, M. Chiba, Nonlinear vibrations of a clamped rectangular plate with initial deflection and initial edge displacement—Part I: theory, Thin-Walled Struct. 1 (1) (1983) 3–29.
[4] N. Yamaki, K. Otomo, M. Chiba, Nonlinear vibrations of a clamped rectangular plate with initial deflection and initial edge displacement—Part II: experiment, Thin-Walled Struct. 1 (2) (1983) 101–119.
[5] D. Hui, Large amplitude axisymmetric vibrations of geometrically imperfect circular plates, J. Sound Vib. 91 (2) (1983) 239–246.
[6] D. Hui, Effects of geometric imperfections on large-amplitude vibrations of rectangular plates with hysteresis damping, J. Appl. Mech. Trans. ASME 51 (1) (1984) 216–220.
[7] H. Eslami, O.A. Kandil, Two-mode nonlinear vibration of orthotropic plates using method of multiple scales, AIAA J. 27 (7) (1989) 961–967.
[8] S. Sassi, G.L. Ostiguy, Analysis of the variation of frequencies for imperfect rectangular plates, J. Sound Vib. 177 (5) (1994) 675–687.
[9] S. Sassi, M. Thomas, F. Laville, Dynamic response obtained by direct numerical integration for pre-deformed rectangular plates subjected to in-plane loading, J. Sound Vib. 197 (1) (1996) 67–83.
[10] D.C. Chen, A.A. Shabana, The rotary inertia effect in the large reference displacement analysis of initially curved plates, J. Sound Vib. 162 (1) (1993) 97–121.

[11] M. Amabili, S. Carra, Thermal effects on geometrically nonlinear vibrations of rectangular plates with fixed edges, J. Sound Vib. 321 (3-5) (2009) 936–954.
[12] D. Hui, Accurate backbone curves for a modified-duffing equation for vibrations of imperfect structures with viscous damping, J. Vib. Acoust. Trans. ASME 112 (3) (1990) 304–311.
[13] G. Singh, G. Venkateswara Rao, N.G.R. Iyengar, Non-linear forced vibrations of antisymmetric rectangular cross-ply plates, Compos. Struct. 20 (3) (1992) 185–194.
[14] M. Amabili, Theory and experiments for large-amplitude vibrations of rectangular plates with geometric imperfections, J. Sound Vib. 291 (3-5) (2006) 539–565.
[15] C. Touzé, C. Camier, G. Favraud, O. Thomas, Effect of imperfections and damping on the type of nonlinearity of circular plates and shallow spherical shells, Math. Probl. Eng. 2008 (2008) https://www.hindawi.com/journals/mpe/2008/678307/.
[16] A. Zarei, A. Khosravifard, Meshfree investigation of the vibrational behavior of pre-stressed laminated composite plates based on a variationally consistent plate model, Eng. Anal. Bound. Elem. 111 (2020) 118–133.
[17] Y.H. Zhou, X.J. Zheng, I.E. Harik, Free-vibration analysis of compressed clamped circular plates, J. Eng. Mech. 121 (12) (1995) 1372–1376.
[18] D. Guojun, L. Huijian, Nonlinear vibration of circular sandwich plate under the uniformed load, Appl. Math. Mech. 21 (2) (2000) 217–226.
[19] G.-j. Du, J.-q. Ma, Nonlinear vibration and buckling of circular sandwich plate under complex load, Appl. Math. Mech. 28 (8) (2007) 1081–1091.
[20] H.-N. Chu, Influence of large amplitudes on flexural vibrations of a thin circular cylindrical shell, J. Aerosp. Sci. 28 (8) (1961) 602–609.
[21] J.C. Chen, C.D. Babcock, Nonlinear vibration of cylindrical shells, AIAA J. 13 (7) (1975) 868–876.
[22] D.C. Chen, A.A. Shabana, Dynamics of initially curved plates in the analysis of spatial flexible mechanical systems, J. Mech. Des. Trans. ASME 115 (3) (1993) 403–411.
[23] E.L. Jansen, Non-stationary flexural vibration behaviour of a cylindrical shell, Int. J. Nonlinear Mech. 37 (4) (2002) 937–949.
[24] O. Thomas, C. Touzé, A. Chaigne, Non-linear vibrations of free-edge thin spherical shells: modal interaction rules and 1:1:2 internal resonance, Int. J. Solids Struct. 42 (11) (2005) 3339–3373.
[25] M. Amabili, Non-linear vibrations of doubly curved shallow shells, Int. J. Nonlinear Mech. 40 (5) (2005) 683–710.
[26] L. Liu, J.-M. Li, G.A. Kardomateas, Nonlinear vibration of a composite plate to harmonic excitation with initial geometric imperfection in thermal environments, Compos. Struct. 209 (2019) 401–423.
[27] M. Shokravi, N. Jalili, Thermal dynamic buckling of temperature-dependent sandwich nanocomposite quadrilateral microplates using visco-higher order nonlocal strain gradient theory, J. Therm. Stress. 42 (4) (2019) 506–525.
[28] M. Amabili, Nonlinear Vibrations and Stability of Shells and Plates, Cambridge University Press, Cambridge, 2008.
[29] H. Takabatake, Effects of dead loads in dynamic plates, J. Struct. Eng. 118 (1) (1992) 34–51.
[30] M. Amabili, Theory and experiments for large-amplitude vibrations of circular cylindrical panels with geometric imperfections, J. Sound Vib. 298 (1) (2006) 43–72.
[31] Y.D. Hu, T. Wang, Nonlinear free vibration of a rotating circular plate under the static load in magnetic field, Nonlinear Dyn. 85 (3) (2016) 1825–1835.
[32] D. Wang, Q. Geng, Y. Li, Effect of static load on vibro-acoustic behaviour of clamped plates with geometric imperfections, J. Sound Vib. 432 (2018) 155–172.
[33] A. Pagani, R. Augello, E. Carrera, Frequency and mode change in the large deflection and post-buckling of compact and thin-walled beams, J. Sound Vib. 432 (2018) 88–104.
[34] E. Carrera, A. Pagani, R. Augello, Effect of large displacements on the linearized vibration of composite beams, Int. J. Nonlinear Mech. 120 (2020) 103390.
[35] E. Carrera, A. Pagani, R. Azzara, R. Augello, Vibration of metallic and composite shells in geometrical nonlinear equilibrium states, Thin-Walled Struct. 157 (2020) 107131.
[36] E. Carrera, A. Pagani, R. Augello, B. Wu, Popular benchmarks of nonlinear shell analysis solved by 1D and 2D CUF-based finite elements, Mech. Adv. Mater. Struct. 27 (13) (2020) 1098–1109.
[37] E. Carrera, G. Giunta, M. Petrolo, Beam Structures: Classical and Advanced Theories, John Wiley & Sons, 2011.
[38] E. Carrera, M. Cinefra, M. Petrolo, E. Zappino, Finite Element Analysis of Structures Through Unified Formulation, John Wiley & Sons, 2014.
[39] S.H. Chen, X.M. Yang, Y.K. Cheung, Periodic solutions of strongly quadratic non-linear oscillators by the elliptic Lindstedt–Poincaré method, J. Sound Vib. 227 (5) (1999) 1109–1118.
[40] H. Hu, Solution of a quadratic nonlinear oscillator by the method of harmonic balance, J. Sound Vib. 293 (1) (2006) 462–468.
[41] H. Hu, Solution of a mixed parity nonlinear oscillator: harmonic balance, J. Sound Vib. 299 (1) (2007) 331–338.
[42] A.Y.T. Leung, Z. Guo, Homotopy perturbation for conservative Helmholtz–Duffing oscillators, J. Sound Vib. 325 (1) (2009) 287–296.
[43] J.-H. He, Homotopy perturbation technique, Comput. Methods Appl. Mech. Eng. 178 (3) (1999) 257–262.
[44] I.A. Yeasmin, N. Sharif, M.S. Rahman, M.S. Alam, Analytical technique for solving the quadratic nonlinear oscillator, Results Phys. 18 (2020) 103303.
[45] J.-w. Zhu, A new exact solution of a damped quadratic non-linear oscillator, Appl. Math. Model. 38 (24) (2014) 5986–5993.
[46] A. Elías-Zúñiga, Analytical solution of the damped Helmholtz–Duffing equation, Appl. Math. Lett. 25 (12) (2012) 2349–2353.
[47] W. Jiang, G. Zhang, L. Chen, Forced response of quadratic nonlinear oscillator: comparison of various approaches, Appl. Math. Mech. 36 (11) (2015) 1403–1416.
[48] A. Gusso, J.D. Pimentel, Approximate fully analytical fourier series solution to the forced and damped Helmholtz–Duffing oscillator, Appl. Math. Model. 61 (2018) 593–603.
[49] Y. Zhou, B. Wu, C.W. Lim, W. Sun, Analytical approximations to primary resonance response of harmonically forced oscillators with strongly general nonlinearity, Appl. Math. Model. 87 (2020) 534–545.
[50] C. Chia, Nonlinear Analysis of Plates, McGraw-Hill International Book Company, 1980.
[51] J.S. Peng, Y.Q. Yuan, J. Yang, S. Kitipornchai, A semi-analytic approach for the nonlinear dynamic response of circular plates, Appl. Math. Model. 33 (12) (2009) 4303–4313.
[52] L. Meirovitch, Analytical Methods in Vibrations, Macmillan, 1967.
[53] S.P. Timoshenko, S. Woinowsky-Krieger, Theory of Plates & Shells, second ed., McGraw-Hill, New York, 1959.
[54] C. Wei-Zang, Large deflection of a circular clamped plate under uniform pressure, Chin. J. Phys. 4 (1947) 102–113.
[55] P. Lin, S.D. Senturia, The in-situ measurement of biaxial modulus and residual stress of multi-layer polymeric thin films, MRS Proc. 188 (1990) 41.
[56] J.-s. Hsu, L.-P. Chao, J.-L. Jhong, T.-F. Chen, W.-C. Tsai, Determining the mechanical properties of optical films in liquid crystal displays (LCDs), Opt. Lasers Eng. 48 (3) (2010) 354–360.
[57] M.G. Allen, S.D. Senturia, Analysis of critical debonding pressures of stressed thin films in the blister test, J. Adhes. 25 (4) (1988) 303–315.
[58] J. Sizemore, R.J. Hohlfelder, J.J. Vlassak, W.D. Nix, Measuring the adhesion of diamond thin films to substrates using the blister test, MRS Proc. 383 (1995) 197.
[59] Y. Zhang, Large deflection of clamped circular plate and accuracy of its approximate analytical solutions, Sci. China Phys. Mech. Astron. 59 (2) (2016) 624602.
[60] M.G. Larson, F. Bengzon, The Finite Element Method: Theory, Implementation, and Applications, 10, Springer Science & Business Media, 2013.
[61] A. Dhooge, W. Govaerts, Y.A. Kuznetsov, H.G.E. Meijer, B. Sautois, New features of the software MATCONT for bifurcation analysis of dynamical systems, Math. Comput. Model. Dyn. Syst. 14 (2) (2008) 147–175.
[62] E.L. Allgower, K. Georg, Introduction to Numerical Continuation Methods, Society for Industrial and Applied Mathematics, 2003.
[63] F. Benedettini, G. Rega, Non-linear dynamics of an elastic cable under planar excitation, Int. J. Nonlinear Mech. 22 (6) (1987) 497–509.
[64] L. Cveticanin, Vibrations of the nonlinear oscillator with quadratic nonlinearity, Phys. A 341 (2004) 123–135.